High electrolyte concentration effect on enzymatic oxygen reduction

Vita Saska, Umberto Contaldo, Ievgen Mazurenko, Anne de Poulpiquet, Elisabeth Lojou

High electrolyte concentration effect on enzymatic oxygen reduction

V. Saska, U. Contaldo, I. Mazurenko, A. de Poulpiquet, E. Lojou*

Aix Marseille Univ, CNRS, BIP, Bioénergétique et Ingénierie des Protéines, UMR 7281, 31, chemin Joseph Aiguier, CS 70071 13402 Marseille cedex 09, France

*Corresponding author : Elisabeth Lojou, lojou@imm.cnrs.fr

ABSTRACT

Nature, composition and concentration of electrolytes is essential for electrocatalysis involving redox enzymes. Different phenomena are expected to drive the efficiency of the process from enzyme conformation, hence stability and activity, to enzyme immobilization at the electrochemical interface. Here, we discuss the effect of various electrolyte composition with increasing ionic strengths on the stability and activity towards O_2 reduction of the bilirubin oxidase from *Myrothecium verrucaria* (*Mv* BOD). Different salts, Na_2SO_4, $(NH_4)_2SO_4$, NaCl, $NaClO_4$, added to a phosphate buffer (PB) were evaluated with concentrations from 100 mM up to 1.7 M. In view of searching for enzyme stabilization, the enzyme was stored in a buffer containing a high salt concentration and the activity was measured in a salt free solution. Opposite to stabilization, we demonstrated that both the homogeneous activity and the electroactivity were decreased. Change in enzyme conformation is most probably at the origin of the decrease of the homogeneous activity, while decrease of the amount of adsorbed enzyme explained the decrease in the electrocatalytic current. Further, the electroactivity was measured in an electrolyte containing increasing salt concentrations. On functionalized carbon nanotube-modified electrodes, which favors functional *Mv* BOD orientation driven by electrostatic interactions, two main effects were observed. On one hand, the catalytic current progressively decreased with increased salt concentrations. On the other hand, the process was reversible suggesting that the decrease in the catalytic current at high ionic strength was not related to enzyme leakage, and that enzyme inactivation at the electrode was also reversible. To get further insight in the phenomenon, the enzyme was immobilized on gold electrodes modified by self-assembling of thiols. Fine examination of the enzyme surface amino acid composition rationalizes the enzyme orientation at the electrode. When the enzyme was simply adsorbed,

the catalytic current decreased in a reversible way, thus behaving similarly than on carbon nanotubes. Enzyme mobility at the interface induced by a modification in the interaction between the protein and the electrode upon salt addition may account for this behavior. When the enzyme was covalently attached, the catalytic current increased, except in the case of NaCl and $NaClO_4$ which inhibited the enzyme. Enzyme compaction is proposed to be at the origin of such catalytic current increase because of shorter distances between the first copper site electron acceptor and the electrode.

KEYWORDS: *Enzyme; Bilirubin oxidase, Catalysis; Electrochemistry; ORR*

1. Introduction

Redox enzymes are attractive for bioelectrochemical devices such as biosensors, bioreactors for bioelectrosynthesis of fine products or biofuel cells [1]. Even if future applications do not necessarily require long-term duration, the poor stability of enzymes and/or of enzyme-based electrodes is an obstacle to large-scale development [2-5]. Strategies exist in order to enhance enzyme stability [6]. In particular, compartmentalization of the biocatalyst into biomatrices or polymers, such as polysaccharides, poly(ethylene glycol), alginate, chitin, or chitosan, has been shown to preserve the native structure of the proteins by providing a more cell-like microenvironment and preventing direct contact of the enzyme with the outside environment [7]. Such enzyme entrapment decreases enzyme conformational dynamic, so that reduced activity is very often the price to pay for enhanced stability. Addition of salts was also proposed to enhance the life time of enzyme. Noticeably, Tsujimura and co-workers recently reported the increased thermostability of glucose dehydrogenase upon addition of salts at concentrations higher than 0.5 M [8]. Different effects depending on the kosmotropicity of the anions were especially highlighted. The role of ionic strength, although not directly discussed in this paper, cannot be ruled out as known to influence interionic interactions in biological systems from change in the degree of ionization of proteins, inducing a change in their conformation and consequently in their biological function to their dehydration, inducing salting out. Otherwise, in bioelectrochemical related processes, electrolyte nature is expected to play key roles [9]. From an electrochemical point of view, the increase in the electrolyte concentration will decrease the ohmic drop effect and will influence the mass transport [10]. From a bioelectrochemical point of view, buffer nature and concentration will have multiple roles, only some being beneficial to bioelectrocatalysis: i) it can act as buffering solution avoiding local pH change deleterious to enzyme activity [11, 12], ii) it may influence enzyme inter-domain

electron transfer [13, 14], iii) it may affect adsorption processes at the electrode and further electrocatalysis, and iv) it may inhibit enzyme activity [15, 16]. Understanding the effect of electrolyte nature, including addition of salts in a buffer solution on bioelectrochemical processes before and after immobilization of enzymes at electrodes is thus all the most important.

Nevertheless, there are not many reports on the effect of buffer nature and concentration on the enzymatic electrocatalysis. Using PB and ammonium sulfate electrolytes at concentrations up to 0.5 M, it was demonstrated a weak impact of the molarity both on MCO stability and activity for O_2 reduction in solution or once the enzyme was immobilized at a graphite microelectrode [17, 18]. On the contrary, increased buffer concentration up to 100 mM and salt addition resulted in enhanced photocurrents from photosystem I immobilized at ITO electrodes [19]. Although not fully elucidated, the effect was attributed to protein conformation changes at the ITO surface. Tsujimura et al. [12] and Kano and co-workers [20] studied the effect of phosphate buffer (PB) concentration on the limited current for enzymatic glucose oxidation. A bell shape relationship between the catalytic current and the ionic strength with the current decreasing once the buffer concentration was higher than 1 M was observed. The process was reversible. The current-buffer concentration dependency was explained by a combination of decrease in the ohmic resistance of the electrolyte, minimization of local pH changes while the decreasing second part was potentially attributed to loss of enzyme activity in solution. When using large surface area electrodes, local pH variation will be even more crucial. In a study combining finite element modeling and electrochemistry, Moore et al. demonstrated pH increase up to 2 units once enzymes such as hydrogenase or formate dehydrogenase are anchored in microporous indium tin oxide electrodes [21]. Proton diffusion limitation could be alleviated by increasing the buffer concentration up to 1 M [20]. A two-rate regime was however highlighted, with decreasing catalytic currents for higher buffer concentrations, enzyme deactivation being hypothesized at the origin of the phenomenon.

Turning to the enzyme immobilization/desorption processes, we extensively reported electrostatic interactions are driving the oriented immobilization of many enzymes, including multicopper oxidases from different origins for an efficient O_2 reduction. In this context, addition of salts into the electrolyte should shield electrostatic interactions, affecting protein orientation before immobilization, amount of immobilized proteins and potential protein desorption from the surface of the electrode. Accordingly, desorption of the laccase from *Trametes versicolor* once immobilized on functionalized carbon nanotubes occurred by addition of increasing amount of $NaHCO_3$ in the electrolyte [22]. Unexpectedly, Badiani et al.

demonstrated that while orientation on the electrode of one hydrogenase and one formate dehydrogenase was driven by electrostatic interactions, salt addition in the buffer up to 3M did not induce desorption of the proteins [23]. The authors suggested the involvement of H-bonding stabilizing the oriented enzyme at the electrode.

From this rapid literature survey, it clearly appears that the relationship between salt concentration or ionic strength of the electrolyte and bioelectrocatalysis is essential but far from being completely understood. Here, we discuss the effect of various electrolyte composition with increasing ionic strengths on the stability and activity towards O_2 reduction of the bilirubin oxidase from *Myrothecium verrucaria*. Different salts, Na_2SO_4, $(NH_4)_2SO_4$, NaCl, $NaClO_4$, added to a phosphate buffer (PB) were evaluated with concentrations from 100 mM up to 1.7 M. High PB concentration was also studied for comparison. We correlate the enzyme activity in solution via spectroscopic measurements using a redox dye to electrocatalytic efficiency displayed by the enzyme wired to an electrochemical interface. Graphite electrodes modified by carbon nanotube films and planar gold electrode modified with two different thiols will allow evaluating the role of the mode of enzyme immobilization, especially physical adsorption or covalent immobilization, on the relationship between high ionic strength electrolytes and enzymatic (electro)catalysis.

2. Experimental

2.1. Materials

BOD from *Myrothecium verrucaria* (*Mv* BOD) was a gift from Amano Enzymes Inc. (Nagoya, Japan). Carboxylic-functionalized carbon nanotubes (CNT-COOH) were purchased from NanoLab Inc. (USA) and dispersions (1 mg/ml) were prepared in Milli-Q water by sonicating for 1 h. Their characterization, including surface chemistry and charge, was previously made in [24]. Ammonium sulfate ($(NH_4)_2SO_4$), sodium sulfate (Na_2SO_4), sodium chloride (NaCl) are from Labbox, Spain. Sodium perchlorate ($NaClO_4$) is from Fluka. 2,2'-azino-bis(3-ethylbenzothiazoline-6-sulphonic acid) diammonium salt (ABTS) (≥98%) and potassium hexacyanoferrate II and III ($K_4[Fe(CN)_6]$ and $K_3[Fe(CN)_6]$) (FeCN) were purchased from Thermo Fisher Scientific and Sigma respectively. 6-mercaptohexanoic acid (6-MHA) and 3,3'-dithiodipropionic acid di(N-hydroxysuccinimide ester) (DTSP) were obtained from Sigma. Phosphate buffer (PB) was used at the concentration of 100 mM and pH 6, unless otherwise specified. Upon addition of high salt concentrations in PB, slight pH variation was balanced by NaOH addition.

2.2. Methods

Spectroscopic assays

Enzymatic assays were performed at 25°C by measuring the absorption at 420 nm using a Cary 60 UV-vis spectrophotometer (Agilent Technologies). ABTS was used as the electron donor. At least three replicates were performed for each condition and the error bars correspond to the standard deviation of the activity. In the cuvette *Mv* BOD and ABTS concentrations were respectively 3 nM and 1.5 mM in 100 mM phosphate buffer pH 6. Enzyme solution with or without salts were stored at 4°C and the activity was measured at regular intervals during 24 h. The catalytic constant (k_{cat}) of *Mv*BOD was calculated by the equation:

$$k_{cat} = \frac{1}{[Enzyme]} \times \frac{1}{60 \times \varepsilon \times L} \times \left(\frac{dAbs}{dt}\right)$$

where ε is ABTS molar absorptivity ($\varepsilon_{420\ nm}$ = 36 mM^{-1} cm^{-1}) and L is the path length (L = 1 cm).

Enzyme aggregation measurement

UV-vis absorptions at 280 nm using an extinction coefficient calculated from the sequence and at 360 nm were carried out at 25°C in 0.1 M phosphate buffer pH 6 without or with 1 M Na_2SO_4 to quantify *Mv* BOD concentrations and aggregate formation respectively. UV-vis spectra were obtained immediately after enzyme preparation (T0), 2 hours later (T2) and after 24 h (T24). Before measurement at 280 nm, all samples including solutions for baselines were centrifuged at 12000 rpm for 10 min. Between the experiments *Mv* BOD solutions were stored at 4°C.

Electrochemistry

Cyclic voltammetry (CV) was performed at 25°C in a standard 3-electrode cell using a potentiostat Autolab PGSTAT30 controlled by 2.1 Nova software (Methrom). A Hg/Hg_2SO_4 reference electrode (sat. K_2SO_4) and a Pt-wire were used as reference and auxiliary electrodes, respectively. All potentials are quoted vs Ag/AgCl (sat. KCl) reference electrode by adding 430 mV to the measured potential. The cell was thermostated at 25 °C and oxygen or nitrogen were continuously bubbled throughout the experiments. 100 mM phosphate buffer pH 6 was used as the electrolyte unless otherwise specified.

Two protocols were used for bioelectrode functionalization. In the first one, a small aliquot (typically 15 µl) of the enzyme solution at a concentration of 1 µM, was drop casted on a graphite electrode (PG, from Bio-Logic Science Instruments, geometric surface area 0.07 cm^2) modified by a film of carbon nanotubes. 5 µl of CNT-COOH at the concentration 1 mg/ml were deposited on the PG electrode. Adsorption of the enzyme was made by incubating the electrode

in the enzyme solution for 15 min at 4°C. Then the bioelectrode was washed with buffer solution to remove loosely bound enzymes, and transferred to the electrochemical cell for electroenzymatic experiments. The capacitive current was measured for each electrode to ensure a reproducibility of the electrode surface is reached. In the second procedure, the enzyme was immobilized on thiol-modified gold electrodes. The gold disc electrodes (from Bio-Logic Science Instruments geometric surface area 0.02 cm^2) were polished for 5 min using alumina slurry 1, 0.3 and 0.04 μm (ESCIL, Lyon France) in the order of decreasing particle size on a fabric polishing pad (PRESI), ultrasonicated in a water-alcohol solution (EtOH:H_2O - 1:1) for 5 min and electrochemically cleaned in a 0.05 M H_2SO_4 solution by cyclic voltammetry till stable and reproducible voltammograms (about 20 cycles) are obtained. Then, the electrodes were washed with Milli-Q water, dried and immediately used for the modification with thiol layers. The electroactive area was measured from the peak area of gold oxide reduction at 0.9 V *vs* Ag/AgCl in 0.05 M H_2SO_4, assuming the charge is equal to 390 $\mu C.cm^{-2}$ [25]. All the currents are reported to the electroactive surface area. For 6-MHA self-assembled-monolayer (SAM), the prepared gold disk electrodes were immersed in freshly prepared 5 mM 6-MHA ethanol solution and left for modification during night. After that, the electrodes were washed with Milli-Q water, air-dried, and used for enzyme immobilization. For DTSP modification, 2 mg of DTSP powder was dissolved in 1 ml of dimethylsulfoxide (DMSO). 5 μl of a freshly prepared aqueous solution of sodium borohydride $NaBH_4$ (10 mg/ml) were added to the DTSP solution, mixed and left for 10 min at room temperature to activate DTSP. After that, the prepared gold electrodes were immersed in 200 μl of the final solution and stored during night at room temperature to form the layer. The electrodes were washed with DMSO, acetone, and Milli-Q water to remove unattached DTSP molecules, air-dried, and used for the immobilization of BOD.[1] 5 μl of 20 μM BOD were immobilized on the surface of the thiol-modified gold electrodes and left in the fridge at 4°C for 15 min.

At least three replicates were performed for each condition and the error bars correspond to the standard deviation of the current.

The following model for irreversible reductive enzymatic catalysis was used to fit the voltametric curves and to evaluate, among other parameters, BOD dispersion of orientations on the electrode [26]:

[1] *Caution: Sodium borohydride decomposes in water producing the hydrogen gas according to the following reaction:* $NaBH_4+2H_2O \rightarrow NaBO_2+4H_2 \uparrow$. *The solution must be used immediately after the preparation and disposed off.*

$$i = \frac{i_{lim}^{red}}{a} \times \left[1 + \frac{1}{\beta d_0} ln \frac{a + \frac{k_{red}}{k_{OR}^0} b}{a + \frac{k_{red}}{k_{OR}^0} b \times \exp(\beta d_0)} \right]$$

Where a and b are defined for a one-electron transition by:

$$a = 1 + e_{OR} = 1 + \exp\left(\frac{F}{RT}\left(E - E_{ox/R}^0\right)\right)$$

$$b = e_{OR}^{\alpha} = e_{OR}^{1/2} = \exp\left(\frac{F}{2RT}\left(E - E_{ox/R}^0\right)\right)$$

i_{lim}^{red} is the value of the reductive limiting current, k_{OR}^0 is the rate constant of electron transfer at zero overpotential for the one-electron conversion O/R, k_{red} is the rate constant of the associated chemical step and $E_{ox/R}^0$ is the formal potential for the one-electron conversion of the T1 copper center. βd_0 is the dispersion parameter, which represents the homogeneous dispersion of enzyme orientations at the electrode surface.

The distribution of enzyme orientations on the electrode surface causes the dispersion in the interfacial electron transfer constant $k_0 \exp(\beta d_0)$ which, among other parameters, depends on the distance of electron tunneling d (the distance between the electrode and the surface exposed redox center which is uniformly distributed between d_{min} and d_{min}+d_0 , hence d_0 is the width of the distance distribution) and β is a decay coefficient. The larger value of βd_0 indicates the larger number of enzyme orientations.

Protein modeling analysis

Molecular graphics and structural analysis were performed with UCSF ChimeraX 1.4 (University of California, USA) [27]. Solvent-exposed amino side chains and coulombic surface analysis of *Mv* BOD were performed using the crystallographic structure (PDB: 2XLL). The crystallographic protein sequence consists of 533 amino-acids residues, the C-terminal Glu_{534} is missing, and the first 38 residues of the DNA sequence are cleaved *in vivo* as post-translational modification [28]. The 533 residues sequence of *Mv* BOD contains a total of 28 arginine and 11 lysine residues as guanidinium group and primary amine side chains, respectively. Of these, 25 arginine and 8 lysine residues are exposed to the solvent on the protein surface. The total solvent accessible surface area (SASA) for these arginine and lysine residues is 1440 and 464 Å^2, respectively, compared with a total surface area of 18509 Å^2. These 33 solvent-accessible residues were classified into three main groups based on their position relative to Cu T1 / TNC, excluding Arg_{147} and the primary amine group Val_1 at the N-terminus.

The relative distances between the guanidinium/amine group and Cu-T1 or TNC were calculated and reported in Table S1. The electrostatic potential surface of *Mv* BOD was calculated according to Coulomb's law. Hydrogen atoms and charge were added in the calculation; histidine was considered biprotonated (pH 6).

3. Results and discussion

3.1. Impact of Na_2SO_4 addition in PB on *Mv* BOD activity and stability in solution

It is well known that salt addition to protein solutions affect the protein solubility and many physicochemical properties, including structural stability. Hofmeister early classified anions and cations according to their ability to precipitate lysozyme [29]. Although still not perfectly understood, it was recognized that ions could also have a stabilizing effect on other proteins according to the Hofmeister series (Scheme S1). More recent works allow to rationalize this effect according to the degree of hydration of ions, and hence to the specific interactions between ions and proteins and between ions and water molecules surrounding the protein [30]. Kosmotropes referred as water-structure formers would tend to stabilize proteins while chaotropes as water-structure breakers would have the opposite effect. Strongly hydrated ions such as SO_4^{2-} (a kosmotrope) tend to strengthen hydrophobic interactions among non-polar amino acid residues resulting in a more compact and spherical enzyme form with smaller surface area, preventing protein dynamics and enhancing stability. Anions were found to have a larger effect than cations because of the larger polarizability they present, a key factor at high salt concentration where electrostatic contribution is screened [29]. Actually, Nemoto et al. recently reported thermostability enhancement of a glucose dehydrogenase by addition of salts in the electrolyte [8]. Their main finding was that Na_2SO_4 and $(NH_4)_2SO_4$ were the two salts able to promote thermostability when used at a concentration higher than 1 M. The enhanced stability was tentatively explained based on the Hofmeister series [8, 31-33].

Based on these published data allowing to envision stabilization of enzymes with time upon salt addition, *Mv* BOD stability was evaluated in solution using classical spectroscopic assays with ABTS as electron donor. 1 µM *Mv* BOD was stored either in 100 mM PB pH 6 or in the same buffer in the presence of 1 M Na_2SO_4. The activity in PB only buffer solution using ABTS assays was realized shortly (less than 5 min) after enzyme dilution (with or without additional Na_2SO_4) and after 6 h and 24 h storage durations at 4°C. These 3 storage duration conditions will be named T0, T6 and T24 respectively. As seen in Figure 1, a remaining activity close to 90% after 24 h of storage at 4°C is obtained when the enzyme is stored in PB only. The addition

of 1 M Na_2SO_4 in the storage solution instead of increasing the stability of *Mv* BOD tends to decrease it, leading to 40% and 60 % loss after 6 h and 24 h of storage respectively. As the assays are realized in PB only solution (whatever the storage solution), the decrease of the activity when the enzyme is stored in the presence of Na_2SO_4 suggests an irreversible process which affects enzyme activity. Similar decrease in activity with storage durations was obtained with $(NH_4)_2SO_4$ (Figure S1). Potential enzyme aggregation upon salt addition, which might be a reason of the activity decline, was evaluated by following absorption at 280 nm with time as a function of buffer composition, i.e. PB without or with 1 M Na_2SO_4. After centrifugation, any decrease in the absorbance will indicate a decrease in the enzyme concentration resulting from aggregate formation and sedimentation. Absorption at 360 nm with time was also followed as an indicator of aggregate formations. As can be seen in Figure S2, almost no concentration change can be detected in PB only over 24 h, whereas 95% of the initial enzyme concentration is remaining in PB + 1 M Na_2SO_4 (Figure S2A). Moreover, few aggregates are formed since the absorbance at 360 nm increases less than 10 % after 24 h of storage whatever the buffer composition (Figure S2B). To explain the activity loss, some irreversible change in the conformation of the enzyme which modifies its affinity with ABTS, hence affects its activity, may occur.

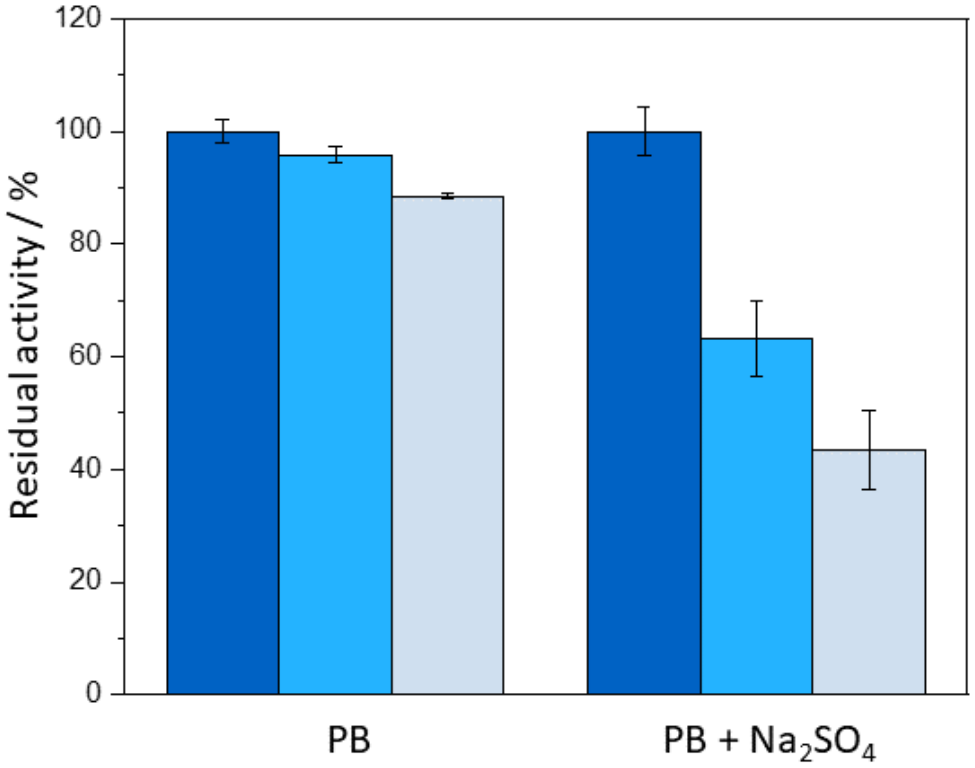

Figure 1. *Mv* BOD activity in solution as a function of enzyme storage duration in PB or PB+ 1 M Na_2SO_4: T0 (dark blue), T6 (light blue), T24 (pale blue). 1 µM BOD solutions were stored at 4°C in 100 mM phosphate buffer pH 6 without or with 1 M Na_2SO_4, and the activity was measured in buffer only solution by spectroscopic assays at 25°C using ABTS as the electron donor.

3.2. Electroactivity of *Mv* BOD stored in solutions containing high salt concentrations

The decrease of homogeneous enzyme activity upon addition of a high amount of salts in the storage solution raises the question of the effect of the solution molarity on the electroactivity of *Mv* BOD for direct O_2 reduction. To evaluate this, we exploited the advantages of CNT-COOH layers expected to enhance both the electroactive surface and the quantity of adsorbed enzymes, hence the catalytic current. In Figure 2A, the typical CVs for direct O_2 reduction by *Mv* BOD deposited at the CNT-COOH-modified PG electrode are depicted. A catalytic wave under O_2, absent under N_2, can be seen when the enzyme comes from the fresh solution which is attributed to direct O_2 reduction by the immobilized BOD. We, and other groups, extensively reported the oriented immobilization of this BOD through electrostatic interactions between the positively charged Cu T1 environment and the negatively charged CNT-COOH surface [4, 34, 35]. The onset potential is 590 mV *vs* Ag/AgCl, a potential expected for *Mv* BOD directly wired, *i.e.* with no redox mediator, through the Cu T1. CV curves recorded with the enzyme stored in PB with 1 M Na_2SO_4 show no difference in shape (Figure 2B). The catalytic currents as a function of storage duration of BOD in phosphate buffer without or with 1 M Na_2SO_4 are depicted in Figure 2C. In the absence of Na_2SO_4 in the buffer, the catalytic current is less than 60% of the initial current after 24 h of *Mv* BOD storage, suggesting that the immobilization step may increase denaturation of already fragilized proteins by a change in their conformation. Upon addition of 1 M Na_2SO_4 in the enzyme solution, two main phenomena can be observed. First the catalytic current at time 0 is decreased being less than 50% of the current observed when *Mv* BOD is stored in PB only. The same observation was made for other redox enzymes such as *T. hirsuta* laccase [36]. Second, catalytic currents after 24 h storage does not highlight stabilization of the enzyme in agreement with UV-Vis measurements. Enzyme aggregation cannot account for this result considering our data showing that about 90% of the enzyme is still available in solution (Figure S2). A decrease of the quantity of adsorbed enzymes and/or an increase in the distribution of orientation of adsorbed proteins is most probably responsible for the decrease in the catalytic current. Indeed, the addition of 1 M Na_2SO_4 in the enzyme

solution will increase the ionic strength (See Table S2 for details), shielding the electrostatic interactions between the electrode and the enzyme solution during the immobilization process [18].

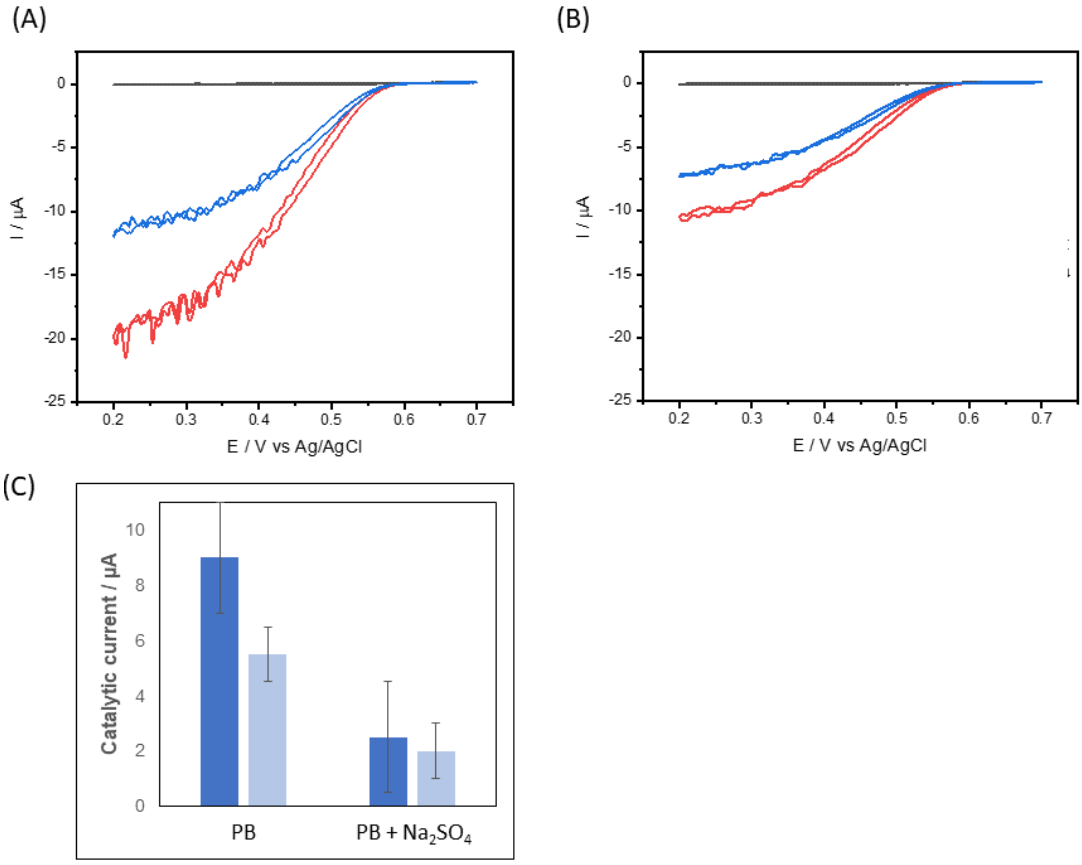

Figure 2. Direct O_2 reduction by *Mv* BOD deposited at CNT-COOH-modified PG electrode as a function of BOD storage duration in 100 mM phosphate buffer pH 6 without or with 1 M Na_2SO_4. (A) CVs using BOD diluted in 100 mM phosphate buffer pH 6 under N_2 (black curve) and O_2 at T0 (red curve) and T24 (blue curve). (B) CVs using BOD diluted in 100 mM phosphate buffer pH 6 + 1 M Na_2SO_4 under N_2 (black curve) and O_2 at T0 (red curve) and T24 (blue curve). (C) Catalytic currents measured at 0.45 V *vs* Ag/AgCl on the CV curves at T0 (dark blue) or T24 (pale blue) without or with 1 M Na_2SO_4 in the enzyme solution. *Mv* BOD was stored at 4°C in 100 mM phosphate buffer without or with 1 M Na_2SO_4 for different durations and then adsorbed on the CNT layer. CVs are performed in 100 mM phosphate buffer pH 6, v = 5 mV/s.

3.3. *Mv* BOD electroactivity on CNT-COOH-modified electrodes in high ionic strength electrolytes

The next step was to evaluate how the bioelectrocatalysis will be influenced by the presence of high salt molarity in the electrolyte. Furthermore, the possibility to renew the electrode surface by simple immersion in high ionic strength electrolyte should be offered by the orientation of *Mv* BOD on the electrode driven by electrostatic interactions. The effect of additional salts in the electrolyte on the direct reduction of O_2 by *Mv* BOD immobilized on an electrochemical interface was thus studied. Figure 3A displays the typical CV curves recorded under O_2 with *Mv* BOD adsorbed onto the CNT-COOH modified electrode with increasing amounts of Na_2SO_4 in the PB electrolyte. The limiting catalytic current decreases by about 50 % after each addition of 1 M (dark blue curve, 45% of the initial current) then 2 M (dark green curve, 24% of the initial current) Na_2SO_4.

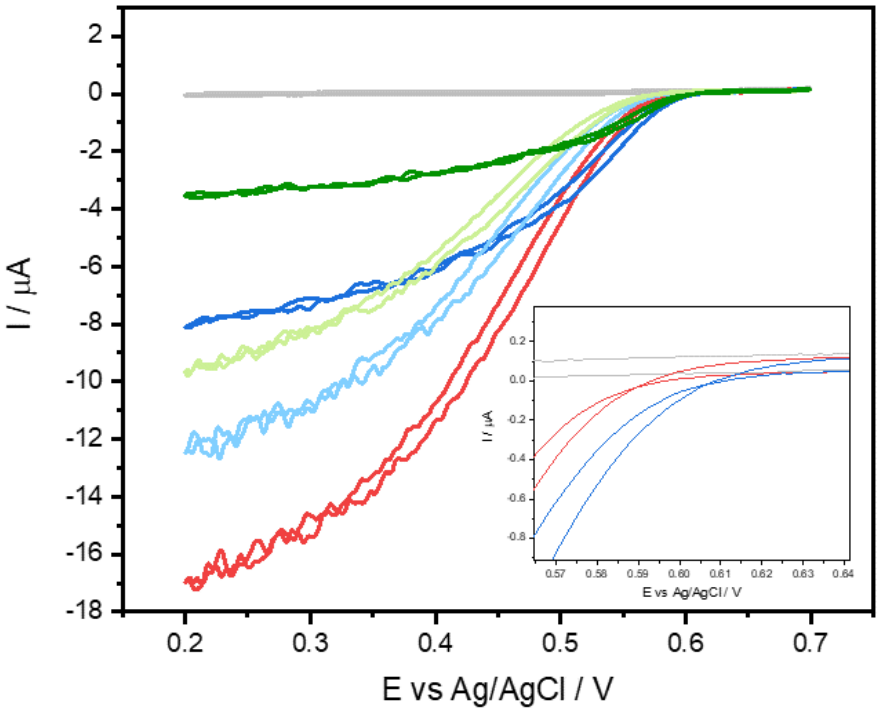

Figure 3. Effect of added Na_2SO_4 in the electrolyte for O_2 reduction by *Mv* BOD adsorbed on CNT-COOH modified electrode. CVs for BOD diluted in 100 mM phosphate buffer pH 6 under N_2 (grey curve), under O_2 (red curve), after addition of 1 M (dark blue curve) and 2 M (dark green curve) Na_2SO_4 addition. Light blue curve and light green curve correspond to transfer back to PB in the sequences 1 M Na_2SO_4→PB and 2 M Na_2SO_4→PB respectively. Insert: Zoom of the CV curves in (A) under O_2 (red curve) and after 1 M Na_2SO_4 addition (dark blue curve) in the potential range 0.64-0.56 V *vs* Ag/AgCl. v = 5 mV/s

To get rid of any influence of the potential cycling on the stability of the bioelectrode, the catalytic current was followed by chronoamperometry at an applied potential of 0.44 V *vs*

Ag/AgCl (Figure 4). As observed with CV, successive additions of Na_2SO_4 from 100 mM up to 1.75 M resulted in a decrease of the catalytic current.

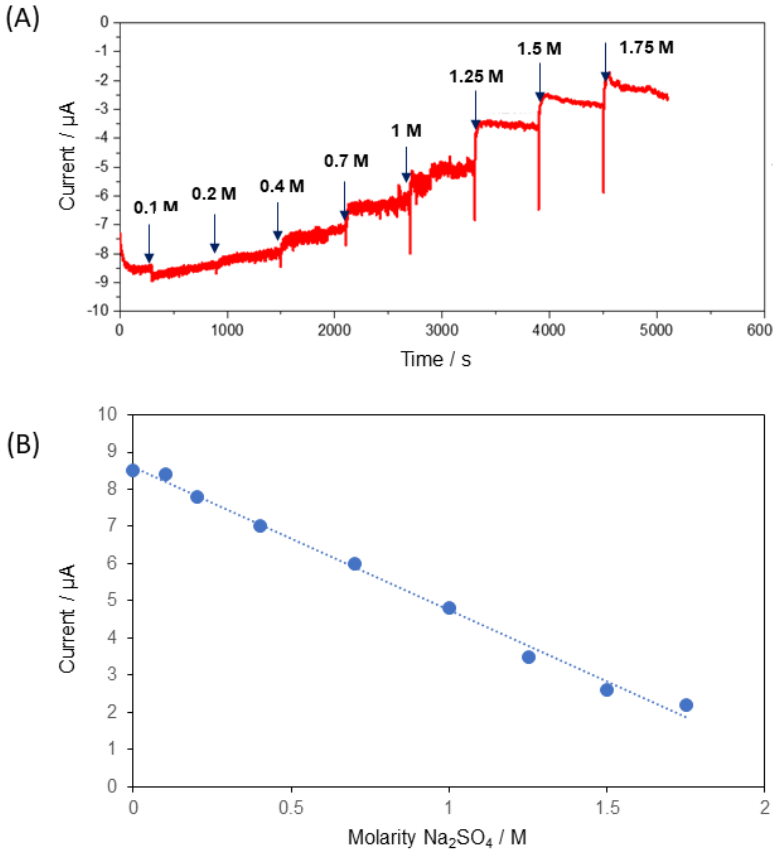

Figure 4. (A) Current recorded in chronoamperometric mode under O_2 at an applied potential 0.44 V *vs* Ag/AgCl with *Mv* BOD immobilized on CNT-COOH modified electrode upon successive additions of Na_2SO_4 in 0.1 M PB pH 6. The final concentration of the salt is indicated with the arrow at the time of injection. (B) evolution of the current as a function of Na_2SO_4 concentration.

Catalytic current decrease induced by salt addition can be linked to enzyme inhibition and/or leakage toward the electrolyte. It must be noted that it was not possible to study the effect of high salt concentrations in the UV-Vis cuvette on the activity of BOD in solution. Actually, in the presence of concentrations of Na_2SO_4 higher than 0.2 M, and in the absence of enzyme, ABTS started to precipitate preventing any reliable activity assays. Nevertheless, the electrochemical signal recorded after each salt addition with the bioelectrode transferred to a salt-free electrolyte provides relevant information. Notably, the catalytic current increases again after this step, being 70% of the initial current after the sequence 1 M Na_2SO_4→PB and 60 %

after the sequence 2 M Na_2SO_4→PB. This result allows first to conclude that there are other significant factors besides desorption that plays role upon salts additions. This also means that other interactions than electrostatic ones are stabilizing the protein on the interface, in agreement with our previous results in 0.5 M PB or 0.5 M $(NH_4)_2SO_4$ [18]. This was also one main finding by Badiani et al. in the cases of formate dehydrogenase and hydrogenase immobilization [23]. As a consequence, despite the fact that enzyme is oriented to the electrode thanks to electrostatic interactions, simple addition of salts in the electrolyte is not efficient for the renewing of the electrode. Second, catalytic current decrease upon salt addition, and recovery of the electrocatalysis upon transfer to a salt free electrolyte signifies that this salt-induced process is reversible.

To be noticed on the inset in Figure 3, an anodic shift of more than 50 mV of the oxygen reduction reaction (ORR) potential was observed when using the electrolyte with added salts. Such a shift was also previously noted when increasing PB or $(NH_4)_2SO_4$ concentration up to 0.5 M and ascribed to enhanced enzyme mobility at the interface [18]. The impact of ionic strength on redox potential was thoroughly studied by Waldeck and Bowden in the case of cytochrome *c* immobilized on various SAMs inducing either adsorbed or covalently attached protein [37]. They identified at least 3 factors that can affect the relationship between redox potential and ionic strength: i) change in the interactions between the charged protein and the charged surface, ii) increased protein desorption with increased ionic strengths, iii) strength of the adsorption, more negative potentials corresponding to stronger binding. The negative shift of the redox potential with decreasing ionic strength at COOH-terminated SAM was explained based on the apparent change in the protein surface charge in interaction with the negatively charged electrode. Such a phenomenon can also explain the shift we recorded with increasing ionic strengths on CNT-COOH.

3.4. *Mv* BOD electroactivity on thiol-modified gold electrodes in high ionic strength electrolytes

CNT layers induce mesoporosity that can influence the effect of salt addition on the electrocatalysis [38]. Thus, to get further insights in the phenomena described above, we investigated the role of salt addition and ionic strength on the electroactivity of *Mv* BOD immobilized on thiol-modified gold surfaces. Two different thiols were used (Scheme 1). 6-MHA was demonstrated to promote the orientation of *Mv* BOD towards the direct wiring of the enzyme through the Cu T1. This was explained by negative charges induced by the SAM at pH 6 which favorably interact with the positively charged environment of Cu T1. DTSP is a

homobifunctional cross-linking reagent containing a cleavable disulfide linkage. A covalent amide bond is formed upon reaction at physiological pH with a primary amine, i.e. surface exposed lysine residues.

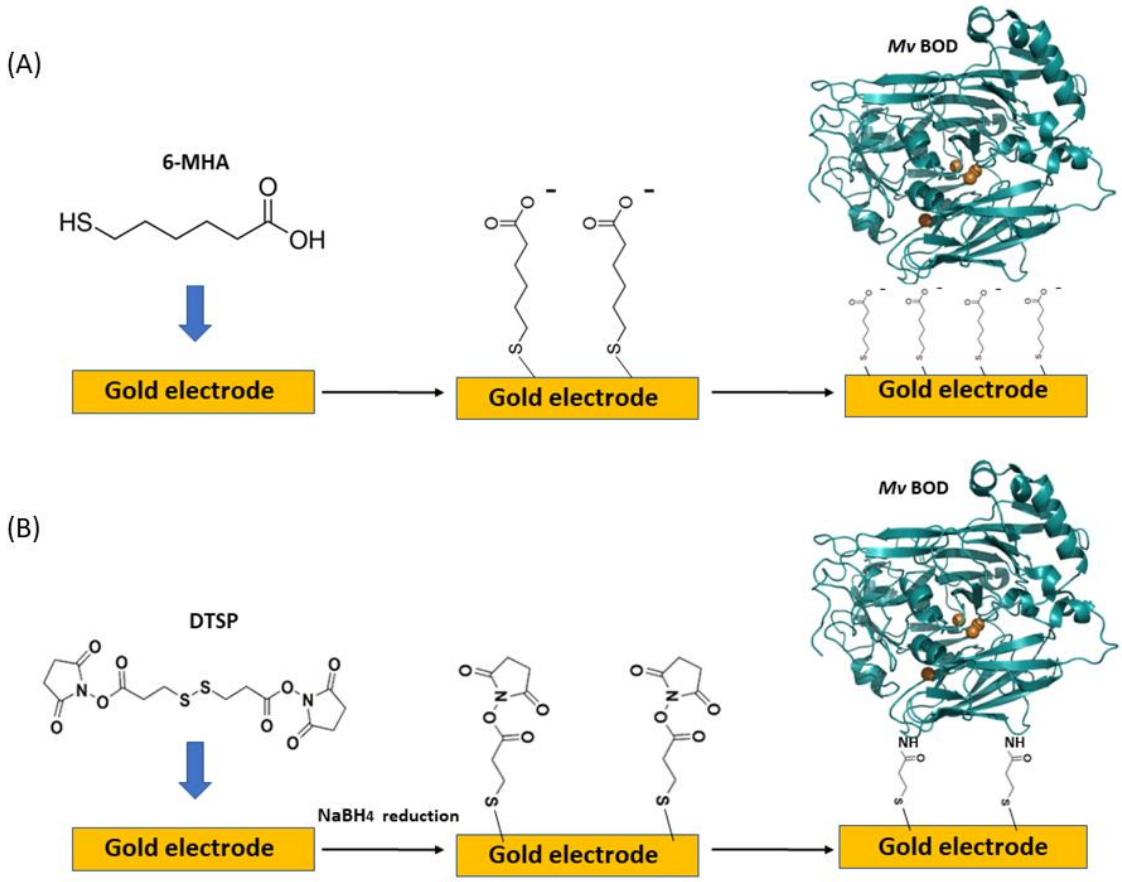

Scheme 1. Thiol-modification of gold electrodes and further *Mv* BOD immobilization with 6-MHA (A) and DTSP (B).

The formation and stability of the two thiol layers were first followed thanks to the electrochemical behavior of the ferricyanide probe. Both thiols blocked the interfacial electron transfer of ferricynanide (Figure S3). From reductive layer desorption in 0.5 M NaOH (Figure S4), a density of thiols on the gold surface of 8.2 10^{-10} and 2.3 10^{-9} mol.cm^{-2} was found for DTSP and 6-MHA respectively, values close to what is expected for thiol monolayers [39, 40]. The stability with time of each layer was confirmed by consecutive cycles in 5 mM ferricynanide solutions and by impedance spectroscopy over 48 h (Figure S5).

The catalytic O_2 reduction induced by the immobilization of *Mv* BOD either by electrostatically driven adsorption on 6-MHA or covalent grafting on DTSP was first studied in PB only electrolyte at pH 6 (Figure 5). In the case of 6-MHA a well-shaped sigmoidal curve is obtained, in agreement with a narrow orientation of BOD (Figure 5A) [5]. Positively charged amino acid

residues, *i.e.* lysine (K) and arginine (R) residues, are mainly found on the surface of the protein (Figure S6). A first cluster of these residues, namely Cluster 1, consists of 9 R and 1 K residues. It is well exposed to the solvent and located near Cu T1 (Table S1). The average distance of these residues (17.4 ± 5.1 Å) to the Cu T1 allows for DET-type catalysis and is responsible for oriented immobilization on negatively charged electrodes such as 6-MHA-modified gold electrode (Figure S7). As for DTSP-electrodes, the covalent linkage involves the binding of primary amines on the protein surface with DTSP (Scheme 1). The lysine residues are mainly present in the Cluster 3 and are too far from Cu T1 for an efficient DET-type catalysis (Figure S6 and Table S1). In agreement, in the case of DTSP, the catalytic current is more than 5 times less the current recorded at 6-MHA-modified gold electrode. The shape of the catalytic signal also reflects a larger distribution of orientations of the enzyme. A parameter βd_0 of enzyme orientation of 4.6±0.11 and 11.3±0.57 for *Mv* BOD on 6-MHA and DTSP respectively was obtained from the fit of the CV curves (Figure S8). To compare the stability induced by the two immobilization methods, chronoamperometry at an applied potential E_{appl} = 0.4 V vs Ag/AgCl was run in 0.1 M PB pH 6 for both electrodes. After 1 hour around 80 % of the catalytic signal was maintained for 6-MHA and DTSP, highlighting similar stability with time in 0.1 M PB, despite very different immobilization mechanism (Figure S9).

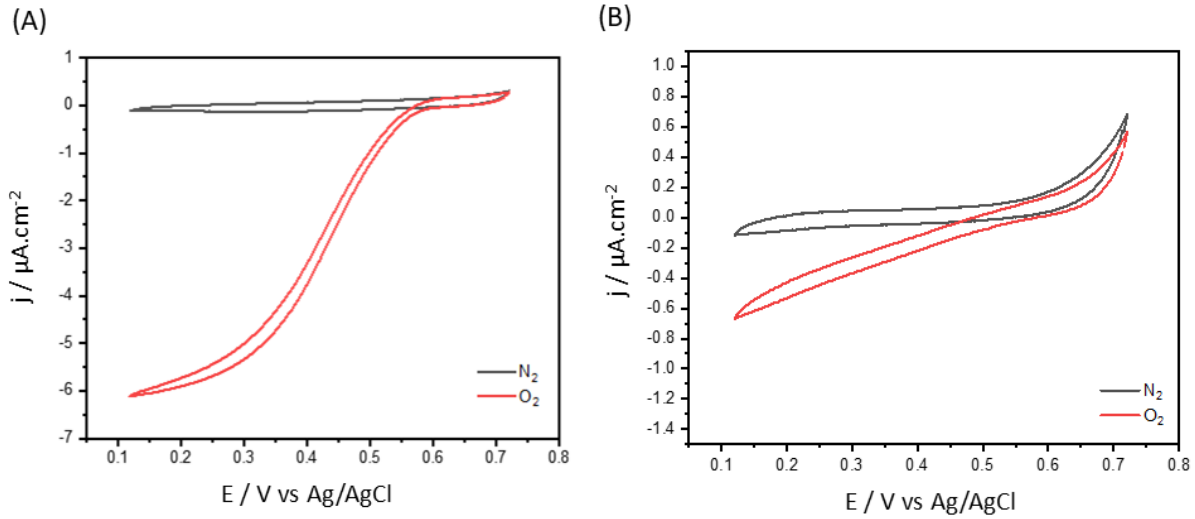

Figure 5. CVs for O_2 reduction (red curves) in 0.1 M PB pH 6 for by *Mv* BOD immobilized on 6-MHA (A) and DTSP (B) layers on gold. In black are the CVs under N_2. v = 5 mV/s.

The evolution of the catalytic current was then followed by chronoamperometry at an applied potential of 0.12 V *vs* Ag/AgCl upon successive additions of Na_2SO_4 from 0.1 up to 1.75 M (Figure 6). In the case of 6-MHA-gold electrode, a decrease of the catalytic current down to values close to 0 was registered, resembled what was observed on CNT-modified electrodes

(Figure 6A). The decrease of the chronoamperometric current is reflected by the CV run just after the chronoamperometry experiment where the limiting current is only 10 % of the initial one. However, as on CNT-modified electrodes, a great recovery of the catalysis is obtained after transfer of the electrode to a salt free PB solution, the limiting current being now more than 80 % of the initial current (Figure 6B). The shape of the voltammogram does not show any significant changes either. The same conclusions as stated for the CNT-based electrode can be drawn: i) decrease in current upon increase of the salt molarity, hence increase in the ionic strength is not linked to enzyme leakage, even when the enzyme is simply immobilized at the interface through electrostatic interaction, ii) salt-induced decrease of the electrocatalysis efficiency is mostly reversible, at least in the case of Na_2SO_4. A very different behavior is observed in the case of DTSP, however. In the range 0-0.4 M Na_2SO_4, the catalytic current remains constant. For highest Na_2SO_4 concentrations, it increases up to 170% of the initial current in the presence of 1.7 M Na_2SO_4 (Figure 6C). The process is reversible since transfer of the DTSP-gold bioelectrode to a salt-free electrolyte induces the recovery of the low initial current (Figure 6D). Various hypothesis can be put forward to explain the evolution of the catalytic current with salt addition depending on thiol-modified gold electrodes: i) Na_2SO_4 induces a reversible inhibition of the enzyme which is prevented upon covalent immobilization of the protein; ii) Na_2SO_4 prevents the direct wiring of *Mv* BOD when it is simply adsorbed on 6-MHA; iii) Na_2SO_4 induces change in the conformation of the enzyme, and potentially affect its flexibility.

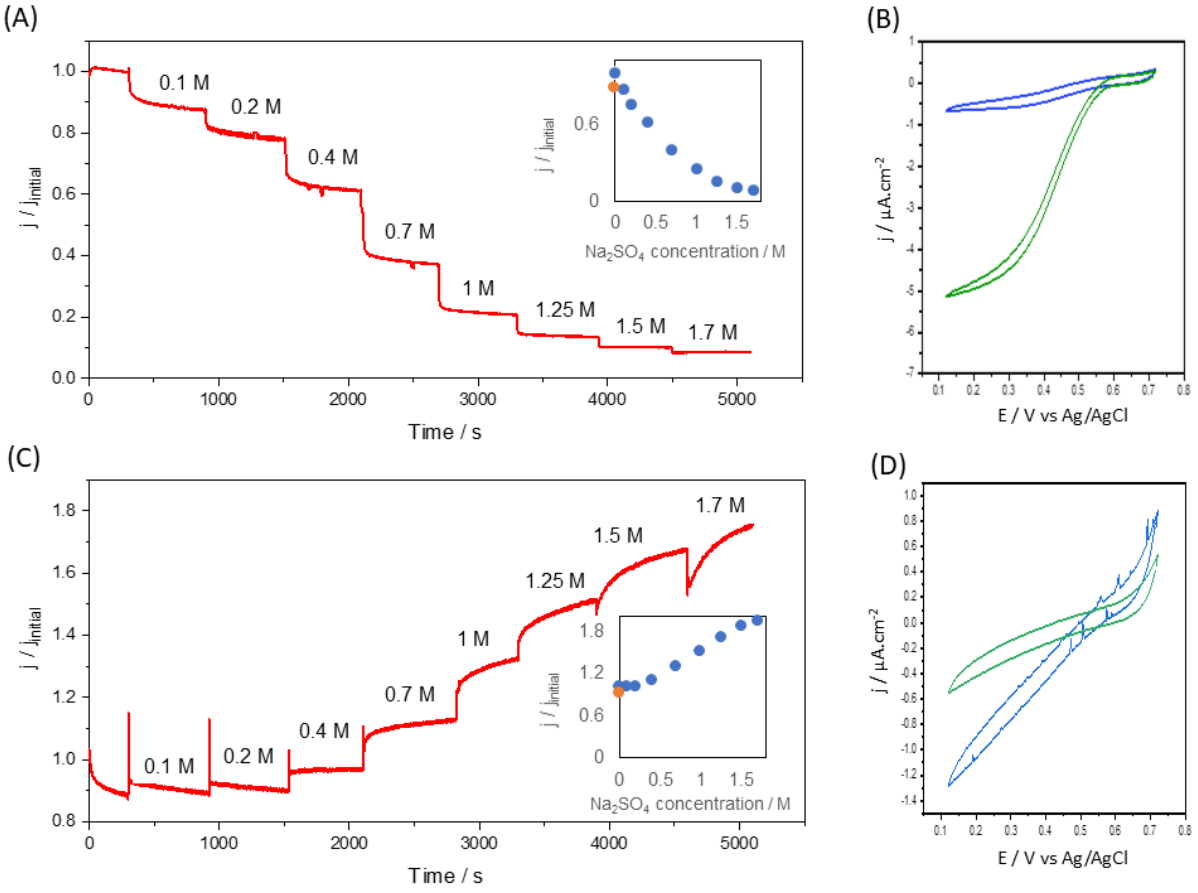

Figure 6. Effect of Na_2SO_4 addition on O_2 reduction by *Mv* BOD immobilized on 6-MHA (A, B) and DTSP (C, D) layer on gold. Chronoamperometric experiments (A, C) were performed at E_{app} = 0.12 V *vs* Ag/AgCl for increasing Na_2SO_4 concentrations from 0.1 M up to 1.7 M in 0.1 M PB pH 6. The inserts in (A) and (C) correspond to the relationship between the ratio of the limiting current to the initial current and the salt concentration. The orange point in the inserts corresponds to the ratio after transfer back of the bioelectrode to a 0.1 M PB. In (B) and (D) are the CVs recorded just after the chronoamperometry (blue curves) and after transfer back of the thiol-modified-bioelectrode into a salt-free PB 0.1 M electrolyte (green curves). v = 5 mV/s.

To assess how widespread the involved processes can be, the effect of other salts than Na_2SO_4 on O_2 reduction by *Mv* BOD immobilized on the two thiol-layers was evaluated. A similar behavior was obtained with increasing amount of $(NH_4)_2SO_4$ instead of Na_2SO_4 (Figure S10): a regular decrease in the catalytic current with increasing amounts of $(NH_4)_2SO_4$ on 6-MHA and an increase in the catalytic current on DTSP. The composition of the two salts will induce the same increase in the ionic strength upon increasing their concentration. Furthermore, both salts are composed of a kosmotropic anion (SO_4^{2-}) associated to a cation whose kosmotropicity

is in the range $NH_4^+ > Na^+$. Cations are however known to have less influence than anions on the protein stability. Moving from NH_4^+ to Na^+ is not expected to have a great impact on protein conformation. The ionic radius of NH_4^+ is however ca. 40% larger than Na^+, suggesting the way they could cause enzyme active center inhibition, if any, should not be the same.

We then examined the effect of electrolytes composed of different anions other than SO_4^{2-}. Halides are largely described inhibitors of MCOs, the extend of inhibition being potential and pH dependent [15, 16]. Although the exact mechanism of inhibition is still missing and seems to be highly dependent on the origin of the MCO, the reversible decrease of the catalytic current was observed once BOD was adsorbed in direct electron transfer orientation on carbon nanostructures [15]. In the present work, we investigated the effect of Cl^- addition in the PB electrolyte on the electrocatalysis for O_2 reduction by *Mv* BOD immobilized on the two thiol layers (Figure 7). A strong effect is observable for Cl^- concentrations much lower than those used for Na_2SO_4. Less than 40% of the activity is maintained after 100 mM NaCl addition, and 1 M NaCl added in 0.1 M PB pH 6, is sufficient to lose the activity of the enzyme immobilized on 6-MHA. The most noticeable feature is the similar decrease in the catalytic current with NaCl addition whatever the thiol-layer used for *Mv* BOD immobilization. The catalytic current in both cases resulting from enzymes directly wired, this indicates that neither 6-MHA nor DTSP prevent chloride to reach the inhibitory site. This result also suggests that the variation in current in the cases of Na_2SO_4 or $(NH_4)_2SO_4$ originates from a different process than occurring with Cl^-.

Although not recognized as a potential MCO inhibitor, our previous reported data showed a decrease in the activity of BOD immobilized on carbon microelectrode in the presence of increasing amount of $NaClO_4$ [11]. The trend observed with $NaClO_4$ in the present work on thiol-modified gold electrodes is very similar to that of NaCl: the addition of only 100 mM $NaClO_4$ induces a decrease in the catalytic current of about 80% and a strong decrease of the catalytic current at high salt concentration occurs no matter of the layer, namely 6-MHA or DTSP (Figure S11). The inhibition is reversible as attested by the recovery of the signal after transfer of the bioelectrode in a salt-free PB.

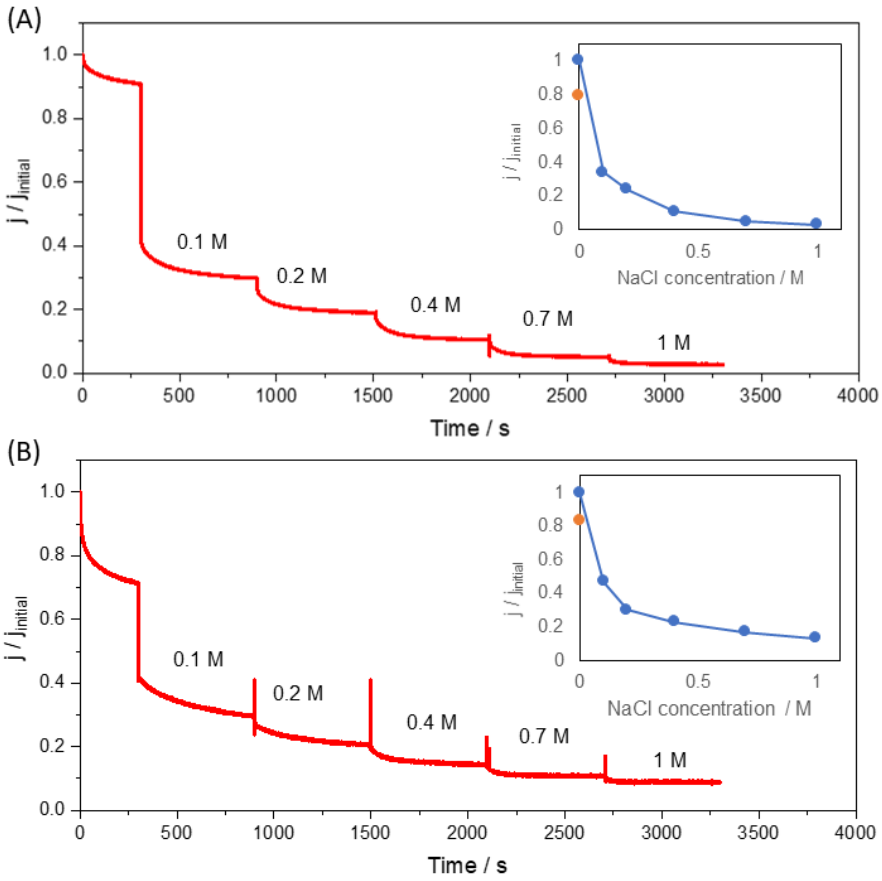

Figure 7. Effect of NaCl addition on O_2 reduction by *Mv* BOD immobilized on 6-MHA (A) and DTSP (B) layers on gold. Chronoamperometric experiments were run at E_{app} = 0.12 V *vs* Ag/AgCl for increasing NaCl concentrations from 0.1 M up to 1 M in 0.1 M PB. The inserts in (A) and (B) correspond to the relationship between the ratio of the limiting current to the initial current and the salt concentration. The orange point in the inserts corresponds to the value of the ratio after transfer back of the bioelectrode to a 0.1 M PB.

Finally, the effect of increasing the concentration of PB itself was evaluated. In order to discriminate between effect of ionic strength or nature of the salts, PB concentration increases were adjusted to fit the ionic strength of each successive addition of Na_2SO_4 (details can be found in Table S2). Due to the limited solubility of KH_2PO_4, concentrations of PB were varied in the range 0.1 to 1.05 M. Chronoamperometric signal for O_2 reduction by *Mv* BOD immobilized either on 6-MHA (Figure 8A) or DTSP (Figure 8B) were followed at an applied potential E_{appl} = 0.12 V *vs* Ag/AgCl. As can be seen, the catalytic current decreases with increasing PB concentrations on both thiol modified-gold electrodes. However, the slope of current decreases with PB concentration is lower in the case of DTSP than for to 6-MHA. At the highest concentration (1.05 M), the catalytic current is 24 % and 75% of the initial current

on 6-MHA and DTSP respectively. On both thiol modified-gold electrodes the process is reversible as the catalytic current measured after transferring back the bioelectrode in 0.1 M PB is 85% and 90 % of the initial current for 6-MHA and DTSP respectively (inserts of Figures 8A and 8B). By increasing PB concentration, we thus confirm a different influence on electrocatalysis depending on whether the protein is adsorbed or covalently bound. It shows again that increasing ionic strength does not induce severe leakage of the protein even when it is immobilized by electrostatic interaction.

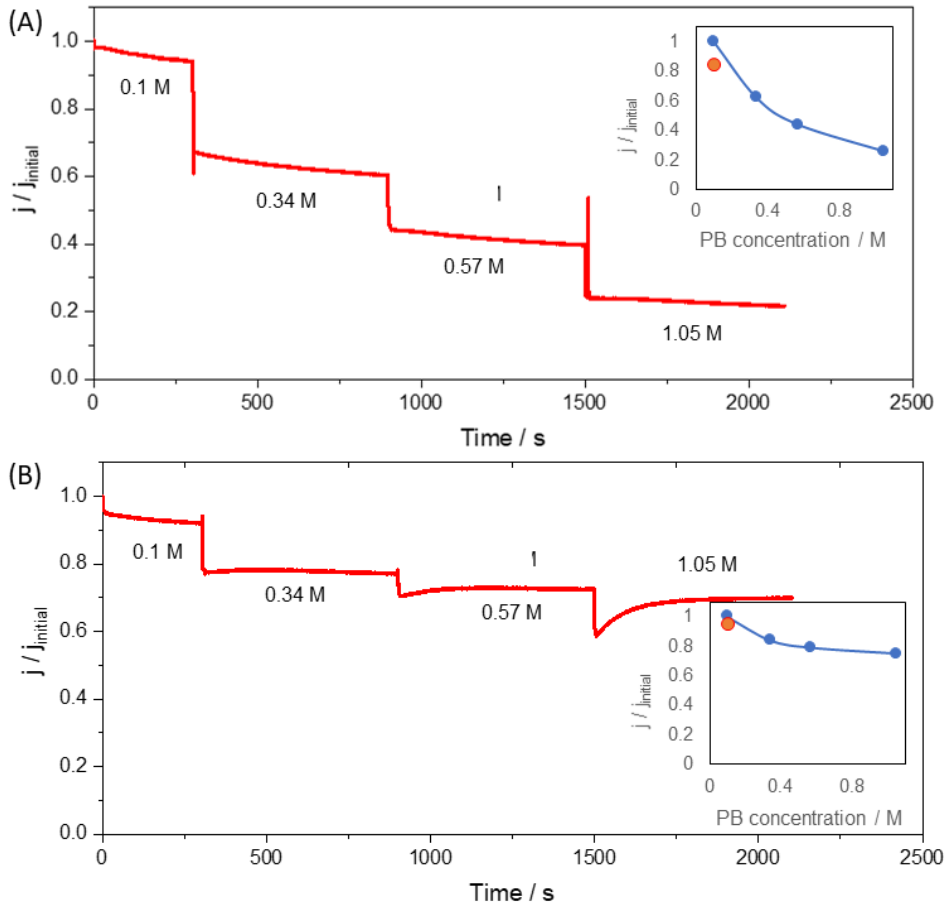

Figure 8. Effect of PB increasing concentration on O_2 reduction by *Mv* BOD immobilized on 6-MHA (A) and DTSP (B) layers on gold. Chronoamperometric experiments were run at E_{app} = 0.12 V *vs* Ag/AgCl for increasing PB concentrations, pH 6, from 0.1 M up to 1.05 M. The inserts in (A) and (B) correspond to the relationship between the ratio of the limiting current to the initial current and the salt concentration. The orange point in the inserts corresponds to the value of ratio after transfer back of the bioelectrode to a 0.1 M PB, pH 6.

4. Concluding remarks

Considering the ensemble of the data obtained at the two thiol-modified electrodes, main comments can be drawn. We will first discuss the cases of Cl^- and ClO_4^- which both induce a strong decrease of the enzymatic activity no matter whether the enzyme is simply adsorbed or covalently grafted. Transfer to a salt-free electrolyte allows recovering the current. In the literature, Cl^- was discussed as an enzyme inhibitor by entering the enzyme channel and binding to the TNC, or approaching the Cu T1 [15, 16, 36, 41-43]. From the data collected in the present work, Cl^- specifically binding to the Cu T1 or in its vicinity cannot be discriminated. Contrary to Cl^-, ClO_4^- has never been reported as a potential inhibitor of multicopper oxidases. Considering the size of ClO_4^-, it was not expected that it behaves similarly as Cl^-. Inactivation by ClO_4^- thus requires further investigation to elucidate the involved process.

The influence of the other salts may reveal a key role of the way the enzyme is immobilized at the electrode. Figure 9 compares the evolution of the catalytic current for O_2 reduction on 6-MHA and DTSP for increasing PB or Na_2SO_4 or $(NH_4)_2SO_4$ concentrations at the same ionic strengths. First, a very different behavior is observed depending on the mode of enzyme immobilization, either adsorbed (case of 6-MHA) or covalently grafted (case of DTSP). This observation suggests that the decrease of the current with these salts is not linked to inhibition but to inactivation induced by a change in the interactions with the electrochemical interface. On 6-MHA where the enzyme is immobilized through electrostatic interactions, the increase in the ionic strength decreases the catalytic electroactivity of the enzyme whatever the nature of the salt, namely PB, Na_2SO_4 or $(NH_4)_2SO_4$ (Figure 9A). Increased mobility of the protein on the interface because of weaker interactions upon increasing ionic strength, hence decrease in the amount of directly wired enzymes, can be an explanation to the decrease in the electroenzymatic activity. In line with this hypothesis, such mobility was previously demonstrated upon pH changes at a SAM-modified electrode [5]. Furthermore, much less inactivation and even activation of *Mv* BOD grafted on DTSP suggests that covalent immobilization of *Mv* BOD prevents its inactivation by high electrolyte concentration, either PB, Na_2SO_4 or $(NH_4)_2SO_4$. Note that varying the ionic strength up to 1.33 M signifies the highest $Na_2(SO)_4$ or $(NH4)_2SO_4$ concentration is only 0.4 M, *i.e.* within molarity range where the increase in the activity is still limited (Figures 6 and S10). This result reinforces the hypothesis of the role of enzyme mobility on the interface on its inactivation by increasing ionic strengths. An alternative explanation to the salt-induced evolution of the catalytic currents may be linked to the fact that SO_4^{2-} is highly kosmotrope and will tend to exclude water from the surface of the protein, inducing its compaction and potentially changing its wiring to the electrode. Decrease of the distance between Cu T1 and the electrode as a result of compaction

can explain the increase of the activity at DTSP-gold electrodes upon salt addition. The effect of ionic strength is notably more pronounced in the case of PB compared to the two other salts, however. Since $H_2PO_4^-$ is less kosmotrop than SO_4^{2-}, kosmotropicity may play a role (Scheme S1). However, it must be noted that the ionic strength was kept constant in order to evaluate the respective role of the ionic strength or the nature of the salt. Concentration of PB is more than twice the concentration of the two other salts at a fixed ionic strength (Table S2). Higher molarity of PB can be the main factor explaining its more pronounced effect. Finally, despite enzyme mobility induced by increased ionic strength, no severe enzyme leakage can be observed whatever the salt added and whatever the electrode used for enzyme immobilization. Salt concentrations as high as 1.7 M cannot desorb the protein immobilized either on 6-MHA SAM or on CNT-COOH. This demonstrates that other interactions than electrostatic ones serve to stabilize the protein at the electrode. Which type of interactions are involved will be investigated in a next future.

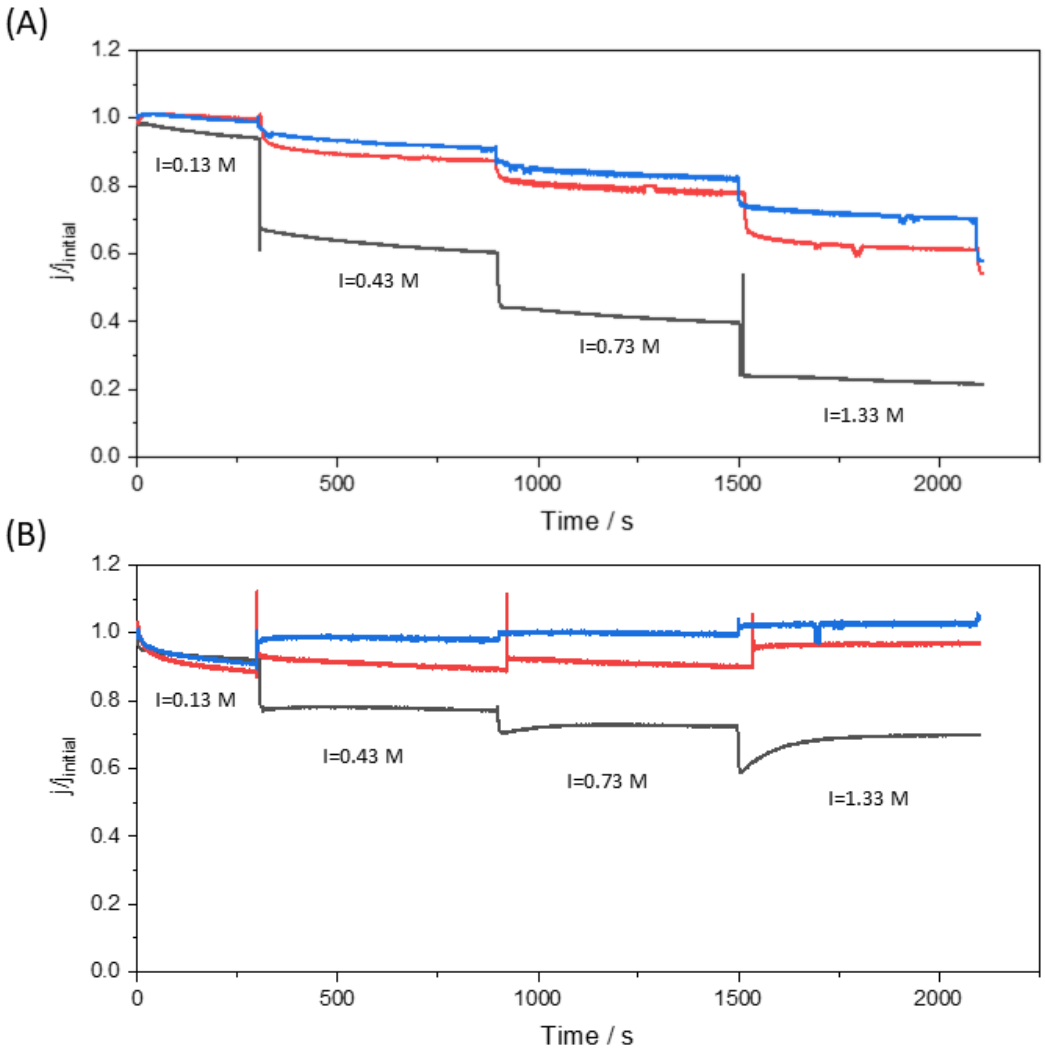

Figure 9. Comparison of the normalized currents recorded during chronoamperometry experiments for O_2 reduction by *Mv* BOD immobilized on (A) 6-MHA and (B) DTSP as a function of the nature of the electrolyte at the same ionic strength noted below the curves for each addition: PB (black curves), Na_2SO_4 (red curves) and $(NH_4)_2SO_4$ blue curves. pH is adjusted to pH 6 and E_{appl} = 0.12 V *vs* Ag/AgCl.

Author contribution

Experiments, V. S.; Enzyme modeling, U C.; Review and editing, A. de P., I. M.; Writing and editing, E. L; Supervision, I. M., E. L.. All authors have read and agreed to the published version of the manuscript.

Acknowledgments

This work was supported by ANR (MetCop-ANR-21-CE44-0024-01). V. S. is grateful to the Institute of Microbiology, Bioenergies and Biotechnology (IM2B, AMX-19-IET-006) and Aix Marseille University for her internship and PhD scholarships.

References

[1] X.X. Xiao, H.Q. Xia, R.R. Wu, L. Bai, L. Yan, E. Magner, S. Cosnier, E. Lojou, Z.G. Zhu, A.H. Liu, Tackling the Challenges of Enzymatic (Bio)Fuel Cells, Chemical Reviews, 119 (2019) 9509-9558.
[2] I. Mazurenko, A. de Poulpiquet, E. Lojou, Recent developments in high surface area bioelectrodes for enzymatic fuel cells, Current Opinion in Electrochemistry, 5 (2017) 74-84.
[3] I. Mazurenko, V.P. Hitaishi, E. Lojou, Recent advances in surface chemistry of electrodes to promote direct enzymatic bioelectrocatalysis, Current Opinion in Electrochemistry, 19 (2020) 113-121.
[4] I. Mazurenko, K. Monsalve, J. Rouhana, P. Parent, C. Laffon, A. Le Goff, S. Szunerits, R. Boukherroub, M.T. Giudici-Orticoni, N. Mano, E. Lojou, How the Intricate Interactions between Carbon Nanotubes and Two Bilirubin Oxidases Control Direct and Mediated O-2 Reduction, Acs Applied Materials & Interfaces, 8 (2016) 23074-23085.
[5] V.P. Hitaishi, I. Mazurenko, M. Harb, R. Clement, M. Taris, S. Castano, D. Duche, S. Lecomte, M. Ilbert, A. de Poulpiquet, E. Lojou, Electrostatic-Driven Activity, Loading, Dynamics, and Stability of a Redox Enzyme on Functionalized-Gold Electrodes for Bioelectrocatalysis, Acs Catalysis, 8 (2018) 12004-12014.
[6] C. Beaufils, H.M. Man, A. de Poulpiquet, I. Mazurenko, E. Lojou, From Enzyme Stability to Enzymatic Bioelectrode Stabilization Processes, Catalysts, 11 (2021).
[7] B. Krajewska, Application of chitin- and chitosan-based materials for enzyme immobilizations: a review, Enzyme and Microbial Technology, 35 (2004) 126-139.
[8] M. Nemoto, K. Sugihara, T. Adachi, K. Murata, K. Shiraki, S. Tsujimura, Effect of Electrolyte Ions on the Stability of Flavin Adenine Dinucleotide-Dependent Glucose Dehydrogenase, Chemelectrochem, 6 (2019) 1028-1031.
[9] C. Carucci, A. Salis, E. Magner, Electrolyte effects on enzyme electrochemistry, Current Opinion in Electrochemistry, 5 (2017) 158-164.
[10] N.G. Tsierkezos, U. Ritter, Influence of concentration of supporting electrolyte on electrochemistry of redox systems on multi-walled carbon nanotubes, Physics and Chemistry of Liquids, 50 (2012) 661-668.

[11] B. Tassy, A.L. Dauphin, H.M. Man, H. Le Guenno, E. Lojou, L. Bouffier, A. de Poulpiquet, In Situ Fluorescence Tomography Enables a 3D Mapping of Enzymatic O-2 Reduction at the Electrochemical Interface, Analytical Chemistry, 92 (2020) 7249-7256.
[12] S. Tsujimura, K. Murata, W. Akatsuka, Exceptionally High Glucose Current on a Hierarchically Structured Porous Carbon Electrode with "Wired" Flavin Adenine Dinucleotide-Dependent Glucose Dehydrogenase, J. Am. Chem. Soc., 136 (2014) 14432-14437.
[13] Z.Y. Xu, J. Zhou, Molecular Insights of Cellobiose Dehydrogenase Adsorption on Self- Assembled Monolayers, Langmuir, 39 (2023) 5880-5890.
[14] P. Bollella, Y. Hibino, K. Kano, L. Gorton, R. Antiochia, The influence of pH and divalent/monovalent cations on the internal electron transfer (IET), enzymatic activity, and structure of fructose dehydrogenase, Analytical and bioanalytical chemistry, 410 (2018) 3253-3264.
[15] A. de Poulpiquet, C.H. Kjaergaard, J. Rouhana, I. Mazurenko, P. Infossi, S. Gounel, R. Gadiou, M.T. Giudici-Orticoni, E.I. Solomon, N. Mano, E. Lojou, Mechanism of Chloride Inhibition of Bilirubin Oxidases and Its Dependence on Potential and pH, Acs Catalysis, 7 (2017) 3916-3923.
[16] M. Valles, A.F. Kamaruddin, L.S. Wong, C.F. Blanford, Inhibition in multicopper oxidases: a critical review, Catalysis Science & Technology, 10 (2020) 5386-5410.
[17] D. Zigah, E. Lojou, A. de Poulpiquet, Micro- and Nanoscopic Imaging of Enzymatic Electrodes: A Review, Chemelectrochem, 6 (2019) 5524-5546.
[18] H.M. Man, I. Mazurenko, H. Le Guenno, L. Bouffier, E. Lojou, A. de Poulpiquet, Local pH Modulation during Electro-Enzymatic O-2 Reduction: Characterization of the Influence of Ionic Strength by In Situ Fluorescence Microscopy, Analytical Chemistry.
[19] S. Morlock, S.K. Subramanian, A. Zouni, F. Lisdat, Bio-inorganic hybrid structures for direct electron transfer to photosystem I in photobioelectrodes, Biosens. Bioelectron., 214 (2022).
[20] H. Sakai, T. Nakagawa, Y. Tokita, T. Hatazawa, T. Ikeda, S. Tsujimura, K. Kano, A high-power glucose/oxygen biofuel cell operating under quiescent conditions, Energy & Environmental Science, 2 (2009) 133-138.
[21] E.E. Moore, S.J. Cobb, A.M. Coito, A.R. Oliveira, I.A.C. Pereira, E. Reisner, Understanding the local chemical environment of bioelectrocatalysis, Proceedings of the National Academy of Sciences of the United States of America, 119 (2022).
[22] S. El Ichi-Ribault, A. Zebda, S. Tingry, M. Petit, A.L. Suherman, A. Boualam, P. Cinquin, D.K. Martin, Performance and stability of chitosan-MWCNTs-laccase biocathode: Effect of MWCNTs surface charges and ionic strength, Journal of Electroanalytical Chemistry, 799 (2017) 26-33.
[23] V.M. Badiani, S.J. Cobb, A. Wagner, A.R. Oliveira, S. Zacarias, I.A.C. Pereira, E. Reisner, Elucidating Film Loss and the Role of Hydrogen Bonding of Adsorbed Redox Enzymes by Electrochemical Quartz Crystal Microbalance Analysis, Acs Catalysis, 12 (2022) 1886-1897.
[24] V.P. Hitaishi, R. Clement, L. Quattrocchi, P. Parent, D. Duche, L. Zuily, M. Ilbert, E. Lojou, I. Mazurenko, Interplay between Orientation at Electrodes and Copper Activation of Thermus thermophilus Laccase for O-2 Reduction, J. Am. Chem. Soc., 142 (2020) 1394-1405.
[25] V.P. Hitaishi, I. Mazurenko, M.A. Vengasseril, A. de Poulpiquet, G. Coustillier, P. Delaporte, E. Lojou, Nanosecond Laser-Fabricated Monolayer of Gold Nanoparticles on ITO for Bioelectrocatalysis, Frontiers in Chemistry, 8 (2020).
[26] V. Fourmond, C. Leger, Modelling the voltammetry of adsorbed enzymes and molecular catalysts, Current Opinion in Electrochemistry, 1 (2017) 110-120.
[27] E.F. Pettersen, T.D. Goddard, C.R.C. Huang, E.E.C. Meng, G.S. Couch, T.I. Croll, J.H. Morris, T.E. Ferrin, UCSF ChimeraX: Structure visualization for researchers, educators, and developers, Protein Science, 30 (2021) 70-82.
[28] J.A. Cracknell, T.P. McNamara, E.D. Lowe, C.F. Blanford, Bilirubin oxidase from Myrothecium verrucaria: X-ray determination of the complete crystal structure and a rational surface modification for enhanced electrocatalytic O-2 reduction, Dalton Transactions, 40 (2011) 6668-6675.
[29] F. Hofmeister, Zur Lehre von der Wirkung der Salze, Archiv für experimentelle Pathologie und Pharmakologie, 24 (1888) 247-260.

[30] B.B. Kang, H.C. Tang, Z.D. Zhao, S.S. Song, Hofmeister Series: Insights of Ion Specificity from Amphiphilic Assembly and Interface Property, Acs Omega, 5 (2020) 6229-6239.
[31] H.I. Okur, J. Hladilkova, K.B. Rembert, Y. Cho, J. Heyda, J. Dzubiella, P.S. Cremer, P. Jungwirth, Beyond the Hofmeister Series: Ion-Specific Effects on Proteins and Their Biological Functions, Journal of Physical Chemistry B, 121 (2017) 1997-2014.
[32] E. Sedlak, D. Sedlakova, J. Marek, J. Hancar, K. Garajova, G. Zoldak, Ion-Specific Protein/Water Interface Determines the Hofmeister Effect on the Kinetic Stability of Glucose Oxidase, Journal of Physical Chemistry B, 123 (2019) 7965-7973.
[33] K. Sakai, Y. Sato, M. Okada, S. Yamaguchi, Enhanced activity and stability of protein-glutaminase by Hofmeister effects, Molecular Catalysis, 517 (2022).
[34] K. Kano, Fundamental insight into redox enzyme-based bioelectrocatalysis, Bioscience Biotechnology and Biochemistry, 86 (2022) 141-156.
[35] A.J. Gross, M. Holzinger, S. Cosnier, Buckypaper bioelectrodes: emerging materials for implantable and wearable biofuel cells, Energy & Environmental Science, 11 (2018) 1670-1687.
[36] C. Vaz-Dominguez, S. Campuzano, O. Rudiger, M. Pita, M. Gorbacheva, S. Shleev, V.M. Fernandez, A.L. De Lacey, Laccase electrode for direct electrocatalytic reduction of O-2 to H2O with high-operational stability and resistance to chloride inhibition, Biosens. Bioelectron., 24 (2008) 531-537.
[37] J. Petrovic, R.A. Clark, H.J. Yue, D.H. Waldeck, E.F. Bowden, Impact of surface immobilization and solution ionic strength on the formal potential of immobilized cytochrome c, Langmuir, 21 (2005) 6308-6316.
[38] I. Mazurenko, K. Monsalve, P. Infossi, M.T. Giudici-Orticoni, F. Topin, N. Mano, E. Lojou, Impact of substrate diffusion and enzyme distribution in 3D-porous electrodes: a combined electrochemical and modelling study of a thermostable H-2/O-2 enzymatic fuel cell, Energy & Environmental Science, 10 (2017) 1966-1982.
[39] N. Zhu, J. Ulstrup, Q.J. Chi, Surface self-assembled hybrid nanocomposites with electroactive nanoparticles and enzymes confined in a polymer matrix for controlled electrocatalysis, Journal of Materials Chemistry B, 3 (2015) 8133-8142.
[40] Q.J. Chi, J.D. Zhang, J.E.T. Andersen, J. Ulstrup, Ordered assembly and controlled electron transfer of the blue copper protein azurin at gold (111) single-crystal substrates, Journal of Physical Chemistry B, 105 (2001) 4669-4679.
[41] R.D. Milton, F. Giroud, A.E. Thumser, S.D. Minteer, R.C.T. Slade, Bilirubin oxidase bioelectrocatalytic cathodes: the impact of hydrogen peroxide, Chemical Communications, 50 (2014) 94-96.
[42] F.A. Al-Lolage, P.N. Bartlett, S. Gounel, P. Staigre, N. Mano, Site-Directed Immobilization of Bilirubin Oxidase for Electrocatalytic Oxygen Reduction, Acs Catalysis, 9 (2019) 2068-2078.
[43] Y. Beyl, D.A. Guschin, S. Shleev, W. Schuhmann, A chloride resistant high potential oxygen reducing biocathode based on a fungal laccase incorporated into an optimized Os-complex modified redox hydrogel, Electrochem. Comm., 13 (2011) 474-476.